INTERNATIONAL JOURNAL OF PRECISION ENGINEERING AND MANUFACTURING Vol. 17, No. 8, pp. 1067-1072 AUGUST 2016 / 1067
DOI: 10.1007/s12541-016-0129-2 ISSN 2234-7593 (Print) / ISSN 2005-4602 (Online)

Optimization for Solid Polymer Microstructure Replication using Gas-Assisted Hot Embossing under Low Pressure

Lei Wan[1], Ning Zhu[1], Xuan Li[1], Rui-ying Zhang[2], and Ting Mei[3,#]

1 Laboratory of Nanophotonic Functional Materials and Devices, Institute of Optoelectronic Material and Technology, South China Normal University, 55, Zhongshan Road West, Guangzhou, 510631, China
2 Key Labs of Nanodevices and Applications, Suzhou Institute of Nano-tech and Nano-bionics, Chinese Academy of Science, 398, Ruishui Road, Suzhou, 215123, China
3 Key Laboratory of Space Applied Physics and Chemistry, Ministry of Education and Shanxi Key Laboratory of Optical Information Technology, School of Science, Northwestern Polytechnical University, 127, Youyi Road West, Xi'an, 710072, China
Corresponding Author / E-mail: ting.mei@ieee.org, TEL: +86-29-88431663, FAX: +86-29-88431664

KEYWORDS: Gas-assisted hot embossing, Polymethylmethacrylate, Structure optimization, Sidewall roughness

In order to realize the replication of high-quality polymer microstructures with vertical and smooth sidewalls, a gas-assisted hot embossing process with low pressure supplied was optimized to eliminate the swallowtail phenomenon during pattern transfer and simplify workpiece process setting. With help of passive alignment clamp, the rate of replication greater than 95.5% for vertical sidewalls was successfully obtained under the optimum process condition. Accordingly, a root mean square sidewall roughness of 4.6 nm was measured for polymer trenches in comparison with that of 5.7 nm for the silicon mold using a bevel-cut preparation technique. Furthermore, the rate of bulging of less than 15% for polymer workpiece was also obtained. The experiment has demonstrated that high-precise polymer pattern replication is related to both process settings and mold morphology sizes.

Manuscript received: September 16, 2015 / Revised: February 28, 2016 / Accepted: April 4, 2016

NOMENCLATURE

T_e = embossing temperature
T_g = glass transition temperature
T_r = demolding temperature
T_o = atmospheric temperature
P_e = embossing pressure
P_o = atmospheric pressure
t = embossing temperature holding time
W_t = top width of trench
W_b = bottom width of trench
D = depth of trench
D = height of vertical sidewall

1. Introduction

With development of micro- and nano- fabrication technologies, embossing polymer has been increasingly adopted as a significant approach of pattern replication. Since it was developed, this technology has been employed in numerous application fields to simplify polymer passive and active devices fabrication including splitter,[1] filter,[2] swithes,[3] modulator,[4] ultrasound detector,[5] laser,[6] bio-chemical sensor, etc. Thus it provides a feasible solution for high-rate development of low-cost polymer photonic devices. For fabricating high-quality patterns on polymethyl methacrylate (PMMA), several innovative plate-to-plate micro-embossing technologies, such as rubber-assisted embossing,[7] ultrasonic-assisted embossing,[8] gas-assisted embossing,[9] etc, have been proposed. The introductions of auxiliary mechanisms have settled some problems, such as fabrication efficiency, pattern uniformity and replication rate, which encountered by the traditional hot embossing technologies. Due to the potential advantages of flexibility of operation, the applicability for complex components, the protection of sheet surface by rubber in terms of rubber pad forming, it has been used to sheet sample molding as a soft substrate embossing tool. Nagarajan and Yao reported the fabrication of shell-type microstructures on thin thermoplastic film using a rubber-assisted embossing process.[10] In order to facilitate polymer filling and demolding during embossing processes, the ultrasonic energy from substrate is converted into heat by virtue of intermolecular friction at the interface between mold and polymer due

to rough surface. Liu et al reported polymer filling acceleration and shortening of process cycle time using an ultrasonic-assisted hot embossing process.[11] Compared with conventional embossing force sources originating from mechanical screw rod or hydraulic drive units, gas pressure can guarantee homogeneous contact between mold and polymer, even if a larger mold is used. Hocheng et al reported good pattern replication uniformity realized using a gas-assisted embossing process.[12] However, as the gas-assisted hot embossing is a non-isothermal process and low pressure is usually supplied, there exists substantial differences between this technology and those traditional embossing technologies in polymer rheological characteristics and workpiece quality inevitably.

Thus far, fabrication of high-precise patterns is still challenging in various hot embossing process approaches. It is known that the pattern fidelity in a hot embossing process is affected by several process parameters, particularly pressure, temperature and time. Generally, a larger pressure is provided to enhance pattern filling,[13-15] but expensive equipment is demanded accordingly. Formation of fine pattern structures mainly depends on polymer filling above T_g. Conformal replication of structures with vertical sidewalls is related to both the polymer viscous flow characteristics and the filling mode.[16] However, inadequate filling is always found in pattern transfer process. Juang et al reported that the curved sidewall profiles were observed for a small cavity thickness (e.g., 1 mm) in isothermal embossing experiments due to the uniform temperature distribution, similar to the results obtained by Yao et al in non-isothermal embossing experiments.[17] To further understand the inherent formation mechanism of this “swallowtail” phenomenon, Liu et al analyzed the deformation behaviors during the stages of ramping and keeping the embossing temperature and pressure in isothermal hot embossing process.[18] And it was concluded that generation of swallowtail was the result of stress concentration and strain hardening. As it is a ubiquitous phenomenon for embossing polymer pattern, process optimization for eliminating swallowtail is of great importance to improving the pattern replication accuracy. Jang et al adopted the segmented pressure ramping during the embossing temperature holding stage to accelerate polymer filling.[19] Oh et al demonstrated that some arcs at the edge line of embossed trenches were improved by increasing the embossing pressure up to 35 bar under an embossing temperature of 140ºC.[20] Moreover, He et al analyzed the embossing process using the finite element method and optimized profile morphology by increasing the embossing temperature holding time to 8 min.[21] However, considering the tradeoff between process parameters and fabrication costs, a simple and efficient process setting is always expected.

In order to further improve pattern replication quality and processing speed under low cost tools, in our work, the optimized silicon wafers with vertical and smooth sidewalls were directly used as embossing molds to replicate polymer pattern in solid PMMA film using a gas-assisted embossing process under a pressure less than 4 kgf/cm^2. The effects of the embossing temperature, the pressure and the embossing temperature holding time on profiles of replicated vertical sidewalls were systematically investigated. A passive alignment clamp was developed to realize simple alignment between embossed polymer and mold, and meanwhile to facilitate polymer filling. The barriers with 250 mm width were fabricated to assist us to directly characterize

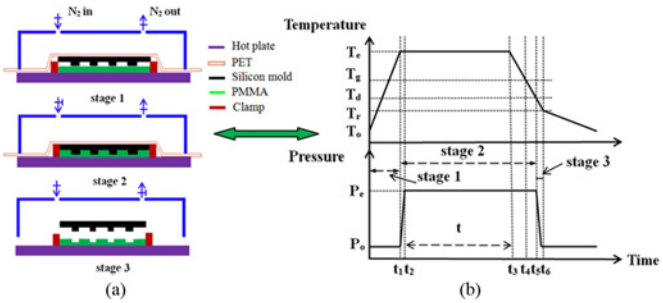

Fig. 1 (a) Stages throughout a complete gas-assisted hot embossing process: (1) temperature ramping (0~t_1), (2) embossing with pressure application and holding (t_1~t_5), (3) decompression and mold releasing (t_5~t_6). (b) The profiles of temperature and pressure at all stages

sidewall roughness of a replicated polymer pattern using the bevel-cut technique.[22] The bulging and thickness reduction of workpieces were compared between one workpiece fixed by clamp and the other without clamp. Finally, the embossed PMMA patterns with vertical and smooth sidewalls were successfully obtained.

2. Experiments

2.1 Preparation for silicon molds

The 2-inch silicon wafers were spin-coated with a 1.4 mm-thick photoresist film (AZ5214), soft baked for 90 s on a hot plate at 95ºC, exposed for 6.8 s on a standard mask aligner system (Karl Suss MA6). The silicon wafers were then developed for 45 s using a developer (3038) in an immersion process, after which, the patterned silicon wafers adhered on a 6-inch silicon wafer using paraffin were etched in an inductively-coupled plasma reactive ion etching (ICPRIE) system (STS Multiplex ASE-HRM) under the optimized condition with 600 W coil source power, 20 W bias power, 130 sccm SF_6 flow rate, 130 sccm C_4F_8 flow rate, and 30 mTorr pressure. The etched silicon wafers were cut into 2×2 cm^2 area using a dicing saw (Disco DAD340) for two types of molds with ridge profiles, mold #1 with 4.56 mm depth and 5.15 mm width and mold #2 with 6.56 mm depth and 5.2 mm width.

In order to reduce the friction between the molds and the embossed material during the mold releasing stage, the silicon molds were deposited with self-assembly fluorine monolayer (SAFM) for 2 h using the thermal evaporation method.[23] The water contact angle for surface-treated silicon molds was increased to 117°, as the feature of highly hydrophobic surface good for the demolding process.

2.2 Gas-assisted hot embossing process

The gas-assisted hot embossing (Gdnano GD-N-02), mainly including three stages, schematically shown in Fig. 1, was employed to fabricate shallow trench microstructures on 1 mm-thick optical PMMA plates. The chamber was separated into two regions by a polyethylene terephthalate (PET) film, the upper for loading pressure with nitrogen and the lower for fastening and heating the workpiece. A simple passive alignment between the embossed polymer and the mold was realized using a clamp depicted in Fig. 2, which was made of metallic aluminum.

Fig. 2 The schematic diagram of the passive alignment clamp for housing the PMMA plate

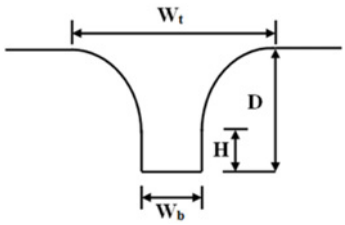

Fig. 3 The characteristics of an embossed polymer trench denoted on the cross-sectional profile

Here the maximum pressure load and the molding temperature were 4 kgf/cm^2 and 300ºC, respectively. Once a lamination was prepared, a gas-assisted hot embossing process would be automatically conducted according to a designed procedure, as presented in Fig. 1(b). For observing cross-sectional deformation of an embossed polymer film, the profile morphology data with defined characteristics were collected from scanning electronic microscopy (SEM) images, as illustrated in Fig. 3.

3. Results and Discussion

Fig. 4 shows the effects of different control parameters including T_e, P_e, and t on characteristic sizes of replicated polymer trenches. It is not difficult to find that D and W_b were not varying much with control parameters while H and W_t gradually approached their counterparts of the mold. But increasing control parameters greatly lessen the swallowtail profile phenomenon. Good conformity of the replicated polymer trench pattern with the mold pattern can be obtained for T_e approaching 170ºC as shown in Fig. 4(a), as the rheological properties of PMMA polymer are sensitive to temperature during embossing process.[24] However, high T_e leads to large adhesion between the mold and polymer material especially for samples fixed by clamp, and thus P_e was increased to boost polymer filling into mold at T_e lower than 170ºC, e.g., 160ºC in Fig. 4(b). The polymer filling was significantly improved for P_e approaching 3.7 kgf/cm^2 as seen in Fig. 4(b), as polymer extensional stress was raised by enhanced squeezing force, causing the melted polymer to flow into free space. Here considering pressure stability, to allow the adoption of a relatively low P_e, e.g., 3 kgf/cm^2, the effect of time extension was investigated in Fig. 4(c). As shown in Figs. 5(a) and (b), the curved edge profiles were increasingly amended with increasing t owing to the combination of enhanced shear flow and extensional flow that fills much more polymer into cavities between

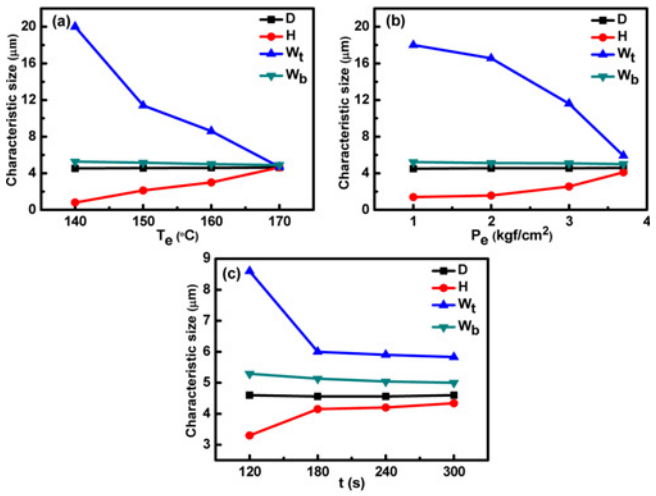

Fig. 4 The characteristic curves of embossed trenches for (a) varying T_e under the condition with P_e=3 kgf/cm^2, t=100 s, and T_r=85ºC, for (b) varying P_e with T_e=160ºC, t=120 s, and T_r=85ºC, for (c) varying t with T_e=160ºC, P_e=3 kgf/cm^2, and T_r=85ºC. The mold #1 was used in experiments

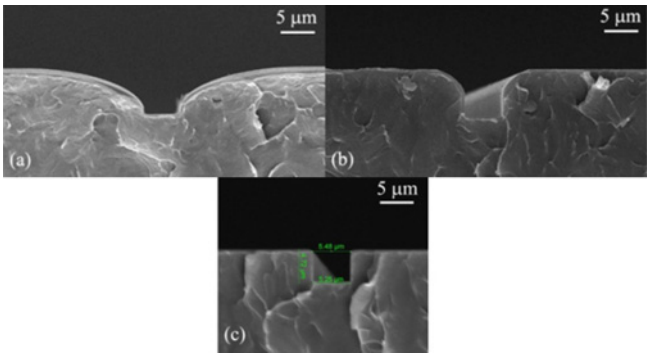

Fig. 5 The SEM images of embossed polymer cross-sectional profiles with T_e=160ºC, P_e=3 kgf/cm^2, T_r=85ºC, and (a) t=0 s, (b) t=60 s, (c) t=300 s

mold features and the PMMA substrate. Such effect on improvement of conformity of the embossed pattern with the mold were significant for embossing holding time up to 180 s only. It was a reason that the polymer stress relaxation was slower than strain hardening with increasing t. In addition, air entrapment existed between mold features and the PMMA substrate also might hinder polymer filling. Therefore, it was reasonable to extend t to push polymer for realizing complete filling. Fortunately, when t increased to 300 s, as presented in Fig. 5(c), the difference value between H and D of embossed trench was only about 0.26 mm, and that between W_t and W_b was about 0.6 mm. As a result, the shape of mold features was well duplicated under the optimized condition with T_e= 160ºC, P_e=3 kgf/cm^2, t=300 s, and T_r=85ºC.

In the paper, the replication rate for vertical sidewalls of embossed trenches was defined as H/D. As shown in Fig. 6, H/D obtained using mold #2 was slightly larger than that using mold #1. The difference value was within 1.5%. It might be demonstrated that there was better thermal conduction for high aspect ratio mold feature in comparison with

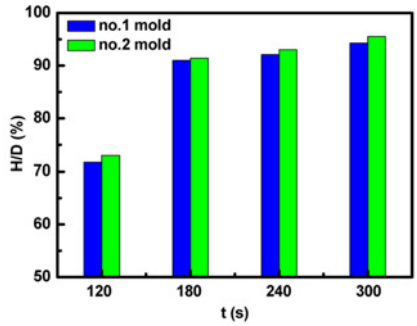

Fig. 6 The comparison of H/D for replication using two molds with clamp at different t

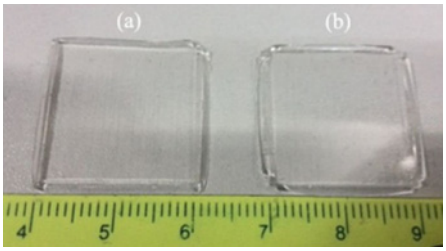

Fig. 7 The photograph of embossed PMMA workpieces (a) without clamp, (b) with clamp

low aspect ratio mold feature because of thermal transmission from the PMMA substrate. Particularly, while t=300 s was applied, H/D was increased to 95.5% for trenches replicated using mold #2. Therefore, it could be inferred that polymer filling was correlated with both process conditions and feature sizes.

The rates of bulging and thickness reduction were referred to in Ref. 12 as 16.67% when the lower PMMA substrate temperature, the upper nickel stamp temperature, P_e and t were set at 80ºC, 150ºC, 22.2 kgf/cm^2 and 300 s, respectively. However, in our experiments depicted in Fig. 7, for the workpiece without clamp, the rate of bulging was 10% when T_e, P_e and t were set at 160ºC, 3 kgf/cm^2 and 300 s, respectively, and the rate of thickness reduction was 13%. For the workpiece with clamp, these values became both 15% with the same process. It illustrated that excessive deformation at the borders of embossed polymer substrate has happened due to high thermal conductivity of metallic aluminum clamp. It is known that sample bulging mainly depended on material original thickness and embossing temperature. Therefore, appropriate process settings are needed to control workpiece size and minimize post-forming treatment, which is conductive to improve processing speed of workpieces.

Before an embossing process was performed, some barriers with 250 mm width were designed in order to directly estimate root mean square (RMS) sidewall roughness using atomic force microscopy (AFM). Once sample with area of 2×2 cm^2 was replicated well, the sample including trenches with width of 250 mm was diced into pieces along a small angle (e.g., 1.4º) from trench side boundary to cutting line. After that, the sidewall profile of embossed trench was exposed with a continuous step barrier in terms of the diced oblique side when

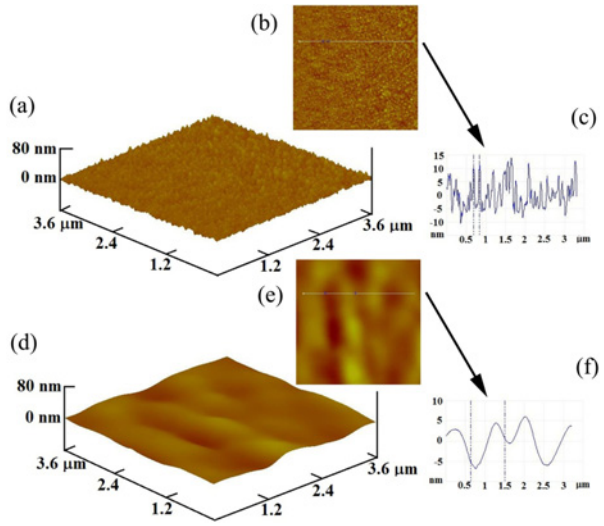

Fig. 8 The morphology images of sidewall roughness. (a) 3-D AFM image, (b) 2-D AFM image, (c) 1-D AFM image for silicon mold and (d) 3-D AFM image, (e) 2-D AFM image, (f) 1-D AFM image for embossed PMMA workpiece

the cross-section of sample was viewed under microscope, which was convenient for AFM tip passing through barrier to scan specific sidewall region. A detailed description is presented in our previous work in Ref. 22. As shown in Fig. 8, the RMS sidewall roughness of 5.7 nm for the silicon mold was measured using a bevel-cut preparation technique. Similar to that, for an embossed polymer workpiece, the RMS sidewall roughness of 4.6 nm in a 3.6×3.6 mm^2 area was obtained. Comparing with Ref. 25, the RMS sidewall roughness of about 20 nm was improved. From the AFM pictures, it was found that large areas of cavities were distributed on etched sidewalls of the silicon mold. The average diameter of cavities for the silicon mold was 150 nm and the maximum depth was about 23 nm. However, this cavities were nearly eliminated in duplicated polymer sidewalls. This is mainly because the polymer filling behavior in the vicinity of sidewalls was restricted by the contact-stress under low pressure supplied. It is demonstrated that with limited polymer viscosity and formability near T_g it was difficult to fill polymer into sub-wavelength structures.[9]

4. Conclusions

In this paper, the profile morphologies of replicated PMMA microstructures with vertical and smooth sidewalls were successfully obtained by optimizing the gas-assisted hot embossing process under the condition with low pressure. In order to remove the swallowtail phenomenon, the effects of T_e, P_e and t on polymer filling behavior were investigated. Based on limited gas pressure supplied, the optimum polymer embossing process with T_e=160ºC, P_e=3 kgf/cm^2, t=300 s, and T_r=85ºC was found for shallow trench fabrication in solid PMMA plate. With help of passive alignment clamp, the rate of polymer filling was slightly accelerated in comparison with that without fixed by clamp. However, the rate of bulging was increased to 15% for workpiece fixed by clamp. By comparing H/D between workpieces replicated by mold

#1 and those by mold #2, it was found that the rate of replication of vertical sidewalls for a large aspect ratio trench was slightly faster than that for a low aspect ratio trench. It was inspiring that a RMS sidewall roughness of 4.6 nm was realized in an embossed PMMA trench using this optimized gas-assisted hot embossing process. Thus, this embossing program is potentially capable of fabricating high-quality polymer waveguide structures.

ACKNOWLEDGEMENT

This work is financially supported by the National Natural Science Foundation of China (grant no. 61176085 & 61377055), the Department of Education of Guangdong Province, China (grant no. gjhz1103) and the open-project funding from Key Labs of Nanodevices and Applications, Suzhou Institute of Nano-tech and Nano-bionics, Chinese Academy of Science, China (grant no. 13ZJ02).

REFERENCES

1. Ryu, J. H., Kim, P. J., Cho, C. S., Lee, E.-H., Kim, C.-S., and Jeong, M. Y., "Optical Interconnection for a Polymeric PLC Device using Simple Positional Alignment," Optics Express, Vol. 19, No. 9, pp. 8571-8579, 2011.
2. Ahn, S.-W., Lee, K.-D., Kim, D.-H., and Lee, S.-S., "Polymeric Wavelength Filter based on a Bragg Grating using Nanoimprint Technique," IEEE Photonics Technology Letters, Vol. 17, No. 10, pp. 2122-2124, 2005.
3. Lin, X., Ling, T., Subbaraman, H., Guo, L. J., and Chen, R. T., "Printable Thermo-Optic Polymer Switches Utilizing Imprinting and Ink-Jet Printing," Optics Express, Vol. 21, No. 2, pp. 2110-2117, 2013.
4. Lin, X., Ling, T., Subbaraman, H., Zhang, X., Byun, K., et al., "Ultraviolet Imprinting and Aligned Ink-Jet Printing for Multilayer Patterning of Electro-Optic Polymer Modulators," Optics Letters, Vol. 38, No. 10, pp. 1597-1599, 2013.
5. Zhang, C., Chen, S.-L., Ling, T., and Guo, L. J., "Review of Imprinted Polymer Microrings as Ultrasound Detectors: Design, Fabrication, and Characterization," IEEE Sensors Journal, Vol. 15, No. 6, pp. 3241-3248, 2015.
6. Ramirez, M. G., Boj, P. G., Navarro-Fuster, V., Vragovic, I., Villalvilla, J. M., et al., "Efficient Organic Distributed Feedback Lasers with Imprinted Active Films," Optics Express, Vol. 19, No. 23, pp. 22443-22454, 2011.
7. Nagarajan, P. and Yao, D., "Rubber-Assisted Micro Forming of Polymer Thin Films," Microsystem Technologies, Vol. 15, No. 2, pp. 251-257, 2009.
8. Peng, L.-F, Deng, Y.-J, Yi, P.-Y., and Lai, X.-M, "Micro Hot Embossing of Thermoplastic Polymers: A Review," Journal of Micromechanics and Microengineering, Vol. 24, No. 1, Paper No. 013001, 2014.
9. Wu, J.-T., Yang, S.-Y., Deng, W.-C., and Chang, W.-Y., "A Novel Fabrication of Polymer Film with Tapered Sub-Wavelength Structures for Anti-Reflection," Microelectronic Engineering, Vol. 87, No. 10, pp. 1951-1954, 2010.
10. Nagarajan, P. and Yao, D., "Uniform Shell Patterning using Rubber-Assisted Hot Embossing Process. I. Experimental," Polymer Engineering & Science, Vol. 51, No. 3, pp. 592-600, 2011.
11. Liu, S. J. and Dung, Y. T., "Hot Embossing Precise Structure onto Plastic Plates by Ultrasonic Vibration," Polymer Engineering & Science, Vol. 45, No. 7, pp. 915-925, 2005.
12. Hocheng, H., Wen, T.-T., and Yang, S.-Y., "Replication of Microlens Arrays by Gas-Assisted Hot Embossing," Materials and Manufacturing Processes, Vol. 23, No. 3, pp. 261-268, 2008.
13. Takagi, H., Takahashi, M., Maeda, R., Onishi, Y., Iriye, Y., et al., "Analysis of Time Dependent Polymer Deformation based on a Viscoelastic Model in Thermal Imprint Process," Microelectronic Engineering, Vol. 85, No. 5, pp. 902-906, 2008.
14. Takagi, H., Takahashi, M., Maeda, R., Onishi, Y., Iriye, Y., et al., "Analysis of Time Dependent Polymer Deformation based on a Viscoelastic Model in Thermal Imprint Process," Microelectronic Engineering, Vol. 85, No. 5, pp. 902-906, 2008.
15. Lee, C.-S., Kang, C.-G., and Youn, S.-W., "Effect of Forming Conditions on Linear Patterning of Polymer Materials by Hot Embossing Process," Int. J. Precis. Eng. Manuf., Vol. 11, No. 1, pp. 119-127, 2010.
16. Juang, Y. J., Lee, L. J., and Koelling, K. W., "Hot Embossing in Microfabrication. Part I: Experimental," Polymer Engineering & Science, Vol. 42, No. 3, pp. 539-550, 2002.
17. Yao, D., Virupaksha, V. L., and Kim, B., "Study on Squeezing Flow during Nonisothermal Embossing of Polymer Microstructures," Polymer Engineering & Science, Vol. 45, No. 5, pp. 652-660, 2005.
18. Liu, C., Li, J. M., Liu, J. S., and Wang, L. D., "Deformation Behavior of Solid Polymer during Hot Embossing Process," Microelectronic Engineering, Vol. 87, No. 2, pp. 200-207, 2010.
19. Ryu, J. H., Lee, T. H., Cho, I.-K., Kim, C.-S., and Jeong, M. Y., "Simple Fabrication of a Double-Layer Multi-Channel Optical Waveguide using Passive Alignment," Optics Express, Vol. 19, No. 2, pp. 1183-1190, 2011.
20. Oh, S. H., Cho, S. U., Kim, C. S., Han, Y. G., Cho, C.-S., and Jeong, M. Y., "Fabrication of Nickel Stamp with Improved Sidewall Roughness for Optical Devices," Microelectronic Engineering, Vol. 88, No. 9, pp. 2900-2907, 2011.
21. He, Y., Fu, J.-Z., and Chen, Z.-C., "Research on Optimization of the Hot Embossing Process," Journal of Micromechanics and Microengineering, Vol. 17, No. 12, pp. 2420-2425, 2007.
22. Wan, L., Li, X., Zhu, N., Zhang, R.-y., and Mei, T., "Optimization for Etching Shallow Ridge and Trench Profiles on Silicon based on

Continuous Etching Process in ICPRIE System," Microsystem Technologies, DOI No. 10.1007/s00542-015-2603-7, 2015.

23. Beck, M., Graczyk, M., Maximov, I., Sarwe, E.-L., Ling, T., et al., "Improving Stamps for 10 nm Level Wafer Scale Nanoimprint Lithography," Microelectronic Engineering, Vols. 61-62, pp. 441-448, 2002.

24. Juang, Y. J., Lee, L. J., and Koelling, K. W., "Hot Embossing in Microfabrication. Part II: Rheological Characterization and Process Analysis," Polymer Engineering & Science, Vol. 42, No. 3, pp. 551-566, 2002.

25. Choi, C.-G., Han, S.-P., Kim, B. C., Ahn, S.-H., and Jeong, M.-Y., "Fabrication of Large-Core 1×16 Optical Power Splitters in Polymers using Hot-Embossing Process," IEEE Photonics Technology Letters, Vol. 15, No. 6, pp. 825-827, 2003.